

Provided for non-commercial research and education use.
Not for reproduction, distribution or commercial use.



Volume 265, Issues 3–4

30 January 2008

ISSN 0012-821X

EARTH & PLANETARY SCIENCE LETTERS



This article was published in an Elsevier journal. The attached copy is furnished to the author for non-commercial research and education use, including for instruction at the author's institution, sharing with colleagues and providing to institution administration.

Other uses, including reproduction and distribution, or selling or licensing copies, or posting to personal, institutional or third party websites are prohibited.

In most cases authors are permitted to post their version of the article (e.g. in Word or Tex form) to their personal website or institutional repository. Authors requiring further information regarding Elsevier's archiving and manuscript policies are encouraged to visit:

<http://www.elsevier.com/copyright>



A 20 ka sediment record from the Hajar Mountain range in N-Oman, and its implication for detecting arid–humid periods on the southeastern Arabian Peninsula

Markus Fuchs^{a,b,*}, Andreas Buerkert^c

^a *Chair of Geomorphology, University of Bayreuth, D-95440 Bayreuth, Germany*

^b *Department of Geology, University of Cincinnati, Cincinnati, OH 45221, USA*

^c *Organic Plant Production and Agroecosystems Research in the Tropics and Subtropics, University of Kassel, D-37213 Witzenhausen, Germany*

Received 8 July 2006; received in revised form 18 October 2007; accepted 19 October 2007

Available online 4 November 2007

Editor: R.W. Carlson

Abstract

Playa-like sediments from the Hajar Mountain range in northern Oman (22.83°N, 59.00°E; 1050 m asl) document variations of the paleoenvironmental and paleoclimate conditions over the last 20 ka. Based on high-resolution sediment sampling and their OSL dating, sedimentation rates were calculated and used as a proxy for paleorainfall. The results show that the Glacial to Lateglacial was characterized by arid conditions with a following transitional period of even less rainfall. At 10.5 ka, sedimentation rates increase abruptly, indicating the onset of the early Holocene humid period (EHHP). Rainfall reaches its maximum at 9–8 ka (EHHP-2) and a decreasing sedimentation rate after 8 ka characterizes the arid period of the middle to late Holocene. Variations of the hydrological regime are associated with the intensity of the boreal summer Indian monsoon and its related position of the ITCZ. For the onset of the EHHP, a northerly shift of the ITCZ is postulated, thus confirming earlier results from the southern Arabian Peninsula.

© 2007 Elsevier B.V. All rights reserved.

Keywords: Indian Ocean Monsoon; climate change; paleoprecipitation; sedimentation rate; luminescence dating; quaternary; Arabia; Oman

1. Introduction

The Indian Ocean Monsoon (IOM) system is one of the major wind systems on earth. It has a global impact on climate and acts as a prominent conveyor belt of heat and

moisture. The IOM dominates the hydrological situation of vast areas in NE-Africa, S-Arabia and India, which has an important impact on the socioeconomic conditions of this region.

The pattern and intensity of the IOM is heavily dependent on the differential heating between the Indian Ocean and the Asian continent. During the boreal summer a low-pressure cell develops over the Tibetan Plateau and a high-pressure cell over the southern Indian Ocean. This causes a northward shift of the Intertropical Convergence

* Corresponding author. Chair of Geomorphology, University of Bayreuth, D-95440 Bayreuth, Germany. Tel.: +49 921 552266/7; fax: +49 921 552314.

E-mail address: markus.fuchs@uni-bayreuth.de (M. Fuchs).

Zone (ITCZ) and generates the SW-Monsoon (Fig. 1). Due to the present-day boreal summer position of the ITCZ along the southern coast of the Arabian Peninsula, only the south-coast areas are affected by the moist SW-Monsoon air masses, whereas further inland arid to hyperarid conditions prevail. In the past, the boreal summer position of the ITCZ fluctuated and during times of a northward shift of the ITCZ, moist air masses penetrated further inland, causing increased precipitation. Based on stable isotope analyses, Weyhenmeyer et al. (2000) could demonstrate that the Indian Ocean was the source of these past moist air masses. On a glacial–interglacial timescale, these continental arid and humid periods are thought to be primarily controlled by glacial boundary conditions (Burns et al., 2001), whereas the influence of the northern hemisphere solar insolation on the position of the ITCZ was demonstrated by Neff et al. (2001).

For the late Quaternary several studies show variations in the pattern and intensity of the IOM, documented in various archives from NE-Africa (Crombie et al., 1997; Gasse, 2000), S-Arabia, (Burns et al., 2001; Glennie and Singhvi, 2002; Preusser et al., 2002; Radies et al., 2004), the Arabian Sea (Sirocko et al., 1993; Leuschner and Sirocko, 2000) and India (Andrews et al., 1998; Juyal et al., 2006). The Holocene–Pleistocene transition for example is marked by an intensification of the IOM with the consequence of a strong increase in early Holocene precipitation. For N-Africa this wet period is well known (DeMenocal, 2000) and recorded by extensive lake deposits (Gasse, 2000; Kröpelin and Soulié-Marsche,

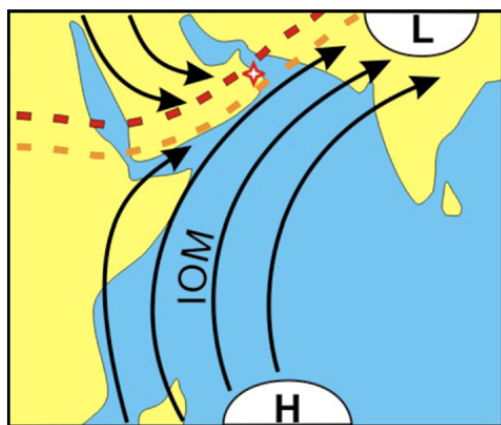


Fig. 1. Generalized map of the low altitude wind pattern during boreal summer time. Dashed orange line represents the nowadays position of the intertropical convergence zone (ITCZ), thus the northern limit of the Indian Ocean Monsoon (IOM) during boreal summer time. Dashed red line is thought to represent the position of the ITCZ during periods of enhanced rainfall over southern Arabia like during the early Holocene moist period (EHHP). The star indicates the location of the study site near the oasis of Maqta. (For interpretation of the references to color in this figure legend, the reader is referred to the web version of this article.)

1991) and flourishing Neolithic civilizations (Kuper and Kröpelin, 2006). For southwest Arabia, Lézine et al. (2007) identified a period of increased precipitation between 12 ka and 7.5 ka recorded by lacustrine sediments in Yemen. Based on faunal assemblages from interdunal deposits in southern Oman, Radies et al. (2005) identified an early Holocene wet period from 9.3 ka to 5.5 ka. Also in a study from southern Oman but based on speleothems, Fleitmann et al. (2003) reported highly depleted $\delta^{18}\text{O}$ values indicating a rapid increase in monsoon precipitation between 10.3 ka and 9.6 ka with a gradual long-term decrease in monsoon precipitation after about 8 ka. Further north at Al Hota cave in the Oman Mountains, a similar onset of the early Holocene pluvial period is indicated by a sudden increase in speleothem growth rates and a drop in calcite $\delta^{18}\text{O}$ at 10.5 ka (Burns et al., 2001). However, the wet period ends at Al Hota cave at 6 ka, thus much later than seen by Fleitmann et al. (2003). Two studies from the United Arab Emirates north of Oman, which are based on dune activities (Bray and Stokes, 2004) and lacustrine geochemistry (Parker et al., 2006), identified the end of the wet period also at 6 ka, even if Parker et al. (2006) reported a much later onset of the wet period at 8.5 ka.

To reconstruct the pattern and intensity of the IOM and its associated position of the ITCZ, the Arabian Peninsula represents a key locality. However, as shown by the discussion about the onset and duration of the early Holocene wet period, the timing of climate fluctuations in southern Arabia is still under debate.

Due to a lack of appropriate climate proxies, paleoclimate reconstruction is not easy in dryland areas and often eolian sediments are used as an indicator of past atmospheric conditions (Chase and Thomas, 2007). However, eolian sediments are a good indicator for dry conditions, but bear only indirect information about past fluctuations in precipitation. In this context, fluvially transported sediments represent a more appropriate proxy for precipitation, and even in dryland areas sediments transported by surface run-off can be found under favorable conditions. This is because the fluvial process plays also in dryland areas an important role in sediment redistribution, which arises from a lack of protecting vegetation cover and infrequent but intensive rainfall, allowing surface run-off with the consequence of fluvial sediment erosion, transportation and its corresponding sedimentation. Thus, if water transported sediments are available, they can be used as a proxy for reconstructing paleohydrological conditions (Eitel et al., 2001, 2005, 2006; Heine 2004).

This paper presents results from a playa-like sediment archive near the oasis of Maqta, situated at the upper end of the Wadi Khabbah in the Jabal Bani Jabir mountains (Hajar range) of northern Oman. Based

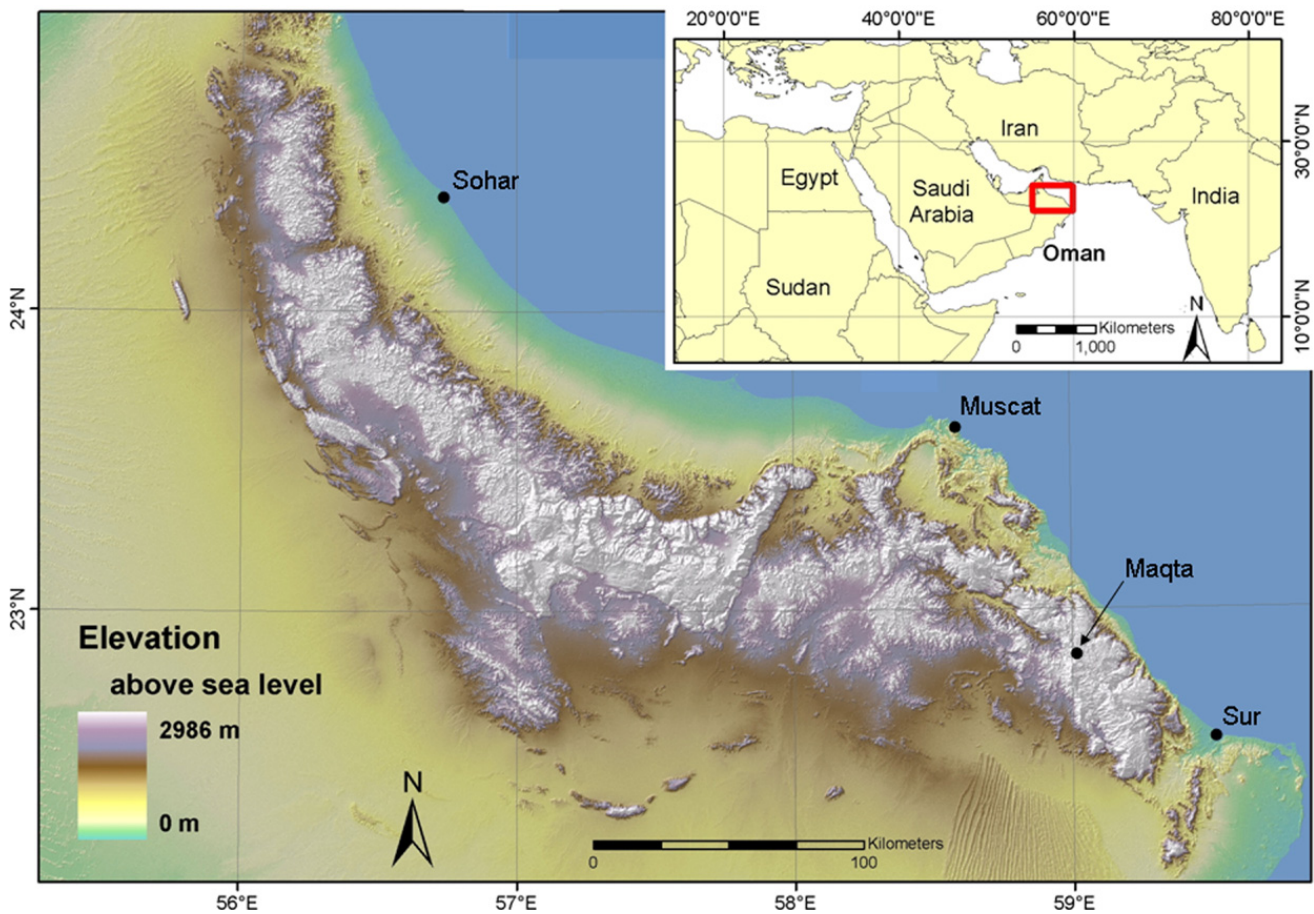


Fig. 2. Position of the oasis of Maqta at the upper end of the Wadi Khabbah of the Jabal Bani Jabir mountains in the Hajar range of northern Oman, southern Arabian Peninsula.

on a 20 m deep sediment profile, the sedimentation history of a sediment-filled depression is reconstructed thereby aiming at shedding some light on the paleoenvironmental and paleoclimate history of the region for the last 20 ka. The chronostratigraphy of the sediment archive was achieved by high-resolution sampling and their optical stimulated luminescence (OSL) dating (Fuchs et al., 2007). Given its unique nature in 2005 the site was revisited to re-sample the sediment profile and to increase the number of OSL samples. While the sediment profile shows a homogeneous structure, marked horizons with rich depositions of mollusk shells and a clear differentiation in the clay contents indicated the possibility to use calculated sedimentation rates and soil chemical properties as a proxy for precipitation in the surrounding catchment area during the late Quaternary period. The main hypothesis of this study therefore was that sedimentation rates of this profile in combination with the soil chemical properties of the profile can be used to deduct precipitation changes as a consequence of fluctuations in the IOM.

2. Study area

The study site is located 150 m above the mountain oasis of Maqta (22.83°N, 59.00°E; 1,050 m asl), on the southwestern flank of the Hajar range in northern Oman (Fig. 2). Here, an ellipsoid shaped, flat depression (ca. 0.5 km²) is situated on a northwest orientated slope (Fig. 3), with its main catchment (ca. 2 km²) upslope to the southeast, characterized by debris covered steep slopes and composed of Cretaceous and Tertiary limestone. The depression is dominantly filled with fine grain sediments of fluvial origin and in its center, grain sizes larger than sand are rare. In contrast, gravel to small boulder size debris is found at the margin of the depression, originating from the adjacent slopes due to mass wasting.

Currently, the study site is located in a mountain desert environment with an average annual rainfall of ca. 50–200 mm falling predominantly in winter time, when cyclonic low-pressure systems from the Eastern Mediterranean (Weyhenmeyer et al., 2000) moving



Fig. 3. The sediment depression near the oasis of Maqta. The arrow indicates the position of the 20 m deep pit in the center of the depression.

across the Arabian Peninsula southward. Farmers' records and own observations during the past eight years indicate that today summer monsoon rainfalls occur only occasionally. As a characteristic of dryland areas, the rainfall is very variable and can be extremely low or even absent for several years. Subsequently, infrequent but heavy thunderstorms can cause intensive rainfall and flooding of the depression for several days (pers. experienced 2005).

The geomorphic system of the depression and its catchment is characterized by a mountainous and non- or only sparsely vegetated desert environment. Physical weathering is the dominant factor controlling *in situ* rock disintegration and clasts of various sizes cover the slopes of the ca. 2 km² catchment. During infrequent but heavy rainfalls surface run-off is generated, which enables the smaller clasts to get washed down the slopes, where the temporarily flowing stream (arroyo) transports the eroded material into the ca. 0.5 km² basin. Here, the material gets accumulated in a shape of a very flat alluvial fan of ca. 1°, dominantly composed of sandy, silty and clayey material. Distal to this fan-like sedimentation zone and in the center of the basin, only fine grain material of dominant clayey and silty material gets accumulated. Due to the character of the sediments and the temporarily flooding of the depression after heavy rainfall events, the term 'playa-like sediments' for the fine grained material accumulated in the center of the basin and distal to the fan-like sedimentation zone is used.

The described fluvial sediment system can be defined as transport-limited with rainfall being the dominant

factor for sediment redistribution. Slope-protecting vegetation cover which would control and reduce erosion is actually absent in the catchment. This is due to the nowadays arid climate conditions with an annual rainfall of 50–200 mm, coupled with a high variability. To establish a protecting vegetation cover, precipitation has to be above 200 mm a⁻¹ and more important with only minor variability. Regional paleoclimate information shows that the last 20 ka were dry (Burns et al., 2001) and only the early Holocene was less dry than today (Fleitmann et al., 2003). However, as shown below, this less dry period is characterized by enhanced sedimentation, thus showing that even during the less dry period, vegetation was not controlling sediment redistribution. Changes in the geomorphometry of the catchment as an additional important factor affecting the sediment redistribution, is thought to be negligible. Studying the geomorphology of the catchment, there were no visible signs indicating a considerable different morphometry of the catchment in the near past.

Because the depression shows no fluvial outlet, the accumulated sediments represent an ideal natural archive for paleoenvironmental studies, with sedimentation rates as a proxy for enhanced or reduced paleorainfall. To investigate the sediments and elucidate the paleoenvironmental and paleoclimate history of the study area, a 20 m deep pit with 1 m in diameter was dug in the center of the depression for profile description and sediment sampling. Due to the size of the catchment, the single inflow to the closed basin and no important sediment sinks between erosion on the slopes and

sedimentation within the basin, the investigated sediment profile seems representative for the fluvio-erosional processes within the catchment.

3. Methods

Sediment samples from the 20 m deep pit were taken from 9 pm to 2 am during two moon-less nights using a rope-ladder of aluminum steps and steel ropes. The dominantly homogeneous sediment profile was continuously sampled at 0.5 m intervals, whereas sampling intervals were adjusted to changing sediment structures in the middle section of the profile. For OSL sampling the profile was carefully cleaned and the samples were directly taken from the pit wall using a scraper and black, light-proof plastic bags.

3.1. Sediment analysis

A first description of the sediment profile was determined in the field. Soil samples were analyzed for their pH in a 1:2.5 0.01 M CaCl₂-suspension, carbonate content (gasometric determination according to Scheibler; VDLUFA, 1991) and organic carbon (C_{org}) according to the Walkley–Black procedure (Page et al., 1982). Soil texture (particle size) was determined by the pipette method (Gee and Bauder, 1986). A total of 39 samples,

comprising 3 cm intervals from 6 to 200 cm profile depth, was analysed for nitrate (NO₃-N), ammonium (NH₄-N) (VDLUFA, 1991) and H₂CO₃-extractable Olsen phosphorus (P; Page et al., 1982).

Because of the limestone characteristic of the fluvial catchment, the quartz content of the samples is thought to be an eolian proxy. Therefore, the quartz content of the samples was semi-quantitatively determined by XRD (Siemens D5005, Siemens AG, Erlangen, Germany), using the ground and decalcified sediment samples.

3.2. Chronostratigraphy

For optical stimulated luminescence (OSL) dating (Aitken, 1998) 35 samples were taken from the exposure. In addition to the 2004 field campaign, the study site was revisited in 2005 to gain (1) new samples from additional depths, and (2) more sample material from the already sampled depths, to re-measure the OSL from samples taken in 2004 (Fuchs et al., 2007).

For OSL measurements, the quartz coarse grain fraction (90–200 μm) was extracted. To this end about 1.5 kg per sample was wet sieved due to the general low quartz content of the sediment. Afterwards, the samples were treated with HCl and H₂O₂ to remove carbonates and organics, followed by heavy liquid density separation with lithium-heteropolytungstate (LST) to separate

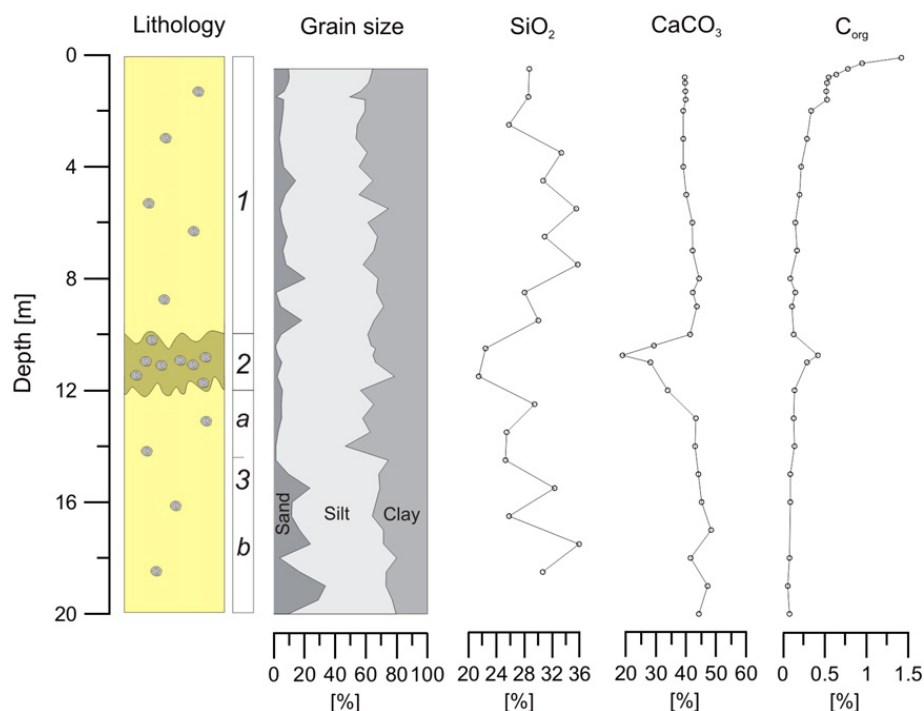


Fig. 4. Sediment succession with their stratigraphical units and analytical data for the profile Maqta. Given are the grain sizes [%] and the contents of SiO₂ [% of the CaCO₃ free fraction], CaCO₃ [%] and C_{org} [%].

Table 1
Sediment analyses

Depth (m)	SiO ₂ (%)	C _{org} (%)	CaCO ₃ (%)
0.1		2.35	
0.3		1.40	
0.5	28.8	1.07	
0.7		0.99	
0.8			39.6
1			39.7
1.1		0.87	
1.3		0.49	39.8
1.5	28.6	0.73	
1.6			39.9
1.7		0.75	
1.9		0.86	
2			39.1
2.1		0.49	
2.5	25.8		
2.6		0.39	
3			39.1
3.4		0.29	
3.5	33.4		
3.9		0.33	
4			39.1
4.5	30.8		
4.8		0.17	
5			40.1
5.5	35.5		
5.8		0.14	
6			42.1
6.5	31.9		
6.8		0.17	
7			42.2
7.25		0.19	
7.5	35.7		
7.75		0.13	
8			44.4
8.35		0.15	
8.5	28.1		42.3
9			43.6
9.16		0.09	
9.5	30.1		
10			41.4
10.3		0.31	
10.4			29.4
10.5	22.5		
10.6		0.24	
10.8			18.9
10.9		0.50	
11			28.2
11.3		0.31	
11.5	21.5		
11.7		0.21	
11.8			
12			33.9
12.3		0.15	
12.5	29.5		
13			43.3
13.3		0.14	
13.5	25.5		

Table 1 (continued)

Depth (m)	SiO ₂ (%)	C _{org} (%)	CaCO ₃ (%)
13.8		0.13	
14			43.0
14.5	25.3		
14.8		0.13	
15			44.1
15.5	32.4		
16			45.2
16.3		0.09	
16.5	25.8		
17			48.4
17.3		0.09	
17.5	35.9		
18			41.5
18.3		0.10	
18.5	30.7		
19			47.2
19.3		0.09	
19.5			
19.8		0.10	
20			44.3

Values for sampling depth, SiO₂, CaCO₃ and C_{org} are listed.

the quartz from any heavy minerals ($>2.75 \text{ g cm}^{-3}$) and feldspars ($<2.62 \text{ g cm}^{-3}$). In the final step, the samples were etched for 1 h in 40% HF to remove the alpha irradiated outer layer of the quartz grains and also to eliminate any potential feldspar contamination. During all steps of the sample preparation, subdued red light ($640 \pm 20 \text{ nm}$) was used.

Luminescence measurements were carried out on a Risø-Reader TL/OSL-DA-15, equipped with blue LEDs ($470 \pm 30 \text{ nm}$) for stimulation and a Thorn-EMI 9235 photomultiplier combined with a 7.5 mm U-340 Hoya filter (290–370 nm) for detection. β -irradiation was performed by a $^{90}\text{Y}/^{90}\text{Sr}$ source ($8.94 \pm 0.4 \text{ Gy min}^{-1}$).

For D_e determination, a single aliquot regenerative dose protocol (SAR) was applied (Murray and Wintle, 2000). Therefore, six regeneration cycles were used and the shine-down curves were measured for 20 s at elevated temperatures (125 °C) after a preheat of 240 °C (10 s) for the natural and regeneration signals and 160 °C for the test dose signals. The integral of 0–0.4 s of the shine-down curves, after subtracting the background signal from the mean of the 16–20 s integral, was used for D_e determination. Feldspar contamination of the aliquots was checked by stimulating the sample with infrared light (IRSL) after artificial dosing. To detect possible insufficient bleaching, all measurements were carried out on small multiple grain aliquots containing ca. 200 grains per aliquots (Fuchs and Wagner, 2003), mounted on aluminum cups (12 mm diameter)

using silicon oil. D_e calculation was based on the measurements of 24 to 100 aliquots per sample, following the procedure suggested by Fuchs et al. (2007).

Low level γ -spectrometry was applied to determine the dose rate (\dot{D}) of the sediments and cosmic-ray dose rates were calculated according to Prescott and Hutton (1994). The water content of the samples was determined using the average value of the possible water content range, based on the porosity of the samples. An error for the water content value was chosen, which included the possible water content range. The values used for the water content were checked by measuring the *in situ* water contents of the samples, showing conformity within errors.

Based on OSL age determinations, sedimentation rates were calculated for every section of the sediment

profile, using a linear regression. The quality of the linear regression is indicated by the coefficient of determination (R^2).

Additionally to the OSL samples, 7 mollusks (*Zootectus insularis*) were sampled for ^{14}C dating from the upper part of the sediment profile. Accelerator mass spectrometry (AMS) measurements were carried out at the Poznań Radiocarbon Laboratory in Poland.

4. Results

4.1. Sediment analysis

Based on the field observations and analytical data, three main sedimentary units were distinguished (Fig. 4

Table 2
Dosimetric data for OSL age calculation

Sample no.	Depth (m)	U (ppm)	Th (ppm)	K (%)	Water content (Δ) ¹	$\dot{D}_{\text{cosm.}}$ (Gy/ka)	\dot{D} (Gy/ka)
BT 110	0.5	2.32±0.17	4.37±0.21	0.92±0.02	1.10±0.05	0.20±0.010	1.80±0.10
BT 84	1.0	3.13±0.09	4.08±0.33	0.88±0.03	1.10±0.05	0.20±0.010	1.91±0.10
BT 111	1.5	3.13±0.08	4.90±0.26	1.01±0.02	1.10±0.05	0.19±0.010	2.07±0.11
BT 96	2.0	2.81±0.09	4.70±0.31	1.01±0.03	1.10±0.05	0.18±0.009	1.99±0.10
BT 112	2.5	3.05±0.09	5.06±0.32	1.05±0.03	1.10±0.05	0.18±0.009	2.10±0.11
BT 69	3.0	2.95±0.09	4.69±0.32	1.00±0.03	1.10±0.05	0.17±0.009	1.99±0.10
BT 113	3.5	2.86±0.07	4.83±0.25	1.05±0.02	1.10±0.05	0.17±0.008	2.02±0.10
BT 114	4.5	2.67±0.07	4.47±0.26	1.12±0.02	1.10±0.05	0.16±0.008	2.01±0.10
BT 85	5.0	2.77±0.09	4.92±0.35	1.12±0.03	1.10±0.05	0.15±0.008	2.06±0.11
BT 115	5.5	2.55±0.09	5.00±0.31	1.12±0.03	1.10±0.05	0.15±0.007	2.01±0.11
BT 116	6.5	2.30±0.08	4.44±0.28	0.98±0.03	1.10±0.05	0.14±0.007	1.78±0.10
BT 99	7.0	2.61±0.07	4.56±0.27	0.98±0.02	1.10±0.05	0.13±0.007	1.85±0.10
BT 117	7.5	2.38±0.06	4.42±0.24	0.94±0.02	1.10±0.05	0.13±0.006	1.76±0.10
BT 86	8.0	2.44±0.07	4.25±0.31	0.90±0.02	1.15±0.07	0.12±0.006	1.64±0.11
BT 118	8.5	2.81±0.07	5.04±0.03	1.15±0.03	1.15±0.07	0.12±0.006	1.97±0.13
BT 119	9.5	2.55±0.06	4.28±0.23	0.95±0.02	1.15±0.07	0.11±0.006	1.69±0.12
BT 101	10.0	2.78±0.08	4.63±0.25	1.07±0.03	1.15±0.07	0.11±0.005	1.86±0.13
BT 120	10.5	3.54±0.11	6.45±0.38	1.44±0.03	1.15±0.07	0.11±0.005	2.43±0.17
BT 155	10.8	3.71±0.14	6.41±0.47	1.38±0.04	1.20±0.07	0.10±0.005	2.30±0.16
BT 121	11.5	3.55±0.10	6.70±0.38	1.45±0.03	1.20±0.07	0.10±0.005	2.34±0.16
BT 102	12.0	2.70±0.09	5.68±0.31	1.25±0.03	1.20±0.07	0.10±0.005	1.95±0.13
BT 122	12.5	2.77±0.08	5.30±0.28	1.67±0.03	1.15±0.07	0.10±0.005	1.97±0.14
BT 103	13.0	2.84±0.06	5.21±0.25	1.16±0.02	1.15±0.07	0.09±0.005	1.97±0.14
BT 123	13.5	2.78±0.07	5.39±0.29	1.23±0.03	1.15±0.07	0.09±0.005	2.02±0.14
BT 104	14.0	2.91±0.08	5.47±0.33	1.17±0.03	1.15±0.07	0.09±0.004	2.00±0.14
BT 124	14.5	2.93±0.06	5.47±0.26	1.21±0.02	1.15±0.07	0.09±0.004	2.03±0.14
BT 105	15.0	2.26±0.06	4.18±0.22	1.01±0.02	1.15±0.07	0.08±0.004	1.65±0.11
BT 125	15.5	2.20±0.08	3.96±0.25	0.92±0.03	1.15±0.07	0.08±0.004	1.55±0.11
BT 106	16.0	2.24±0.08	4.38±0.28	1.07±0.03	1.15±0.07	0.08±0.004	1.70±0.12
BT 126	16.5	2.44±0.08	4.09±0.28	0.91±0.02	1.15±0.07	0.08±0.004	1.59±0.11
BT 107	17.0	2.20±0.07	3.75±0.25	0.87±0.03	1.15±0.07	0.07±0.004	1.49±0.11
BT 127	17.5	2.22±0.07	4.00±0.26	0.92±0.03	1.15±0.07	0.07±0.004	1.54±0.11
BT 128	18.5	2.13±0.06	3.93±0.21	0.81±0.02	1.15±0.07	0.07±0.003	1.42±0.10
BT 109	19.0	2.12±0.07	3.44±0.23	0.80±0.02	1.15±0.07	0.07±0.003	1.38±0.10
BT 129	19.5	2.08±0.06	3.79±0.22	0.93±0.02	1.15±0.07	0.07±0.003	1.51±0.11

Sample no., U-, Th-, and K-contents are based on low-level γ -spectrometry, water content Δ represents the ratio of the wet sample weight to dry sample weight, cosmic dose rate ($\dot{D}_{\text{cosm.}}$) and effective dose rate (\dot{D}) are listed.

¹ Ratio wet sample weight to dry sample weight.

and Table 1). The lower part of the section (unit 3) from 20 m to 12 m is characterized by a homogenous light brown sediment (7.5YR6.3; Munsell Color Corporation 1976) with a calcium carbonate content (CaCO_3) of 42–48% and a SiO_2 content of the carbonate-free sediment fraction of 25–36%. Because of a change in the clay content in favor of the sand fraction at ca. 14 m depth, unit 3 is subdivided in an upper more clayey subunit 3a, and a lower sandier subunit 3b. This subdivision is confirmed by a difference in the C_{org} content, with $\leq 0.1\%$ in subunit 3b and $>0.14\%$ in subunit 3a. Mollusk remains of *Z. insularis* are in places all over unit 3.

Above unit 3 follows unit 2 at 12 m depth with a gradual but distinct change in color (brown, 7.5YR5.3) and a sudden increase in mollusk remains (*Z. insularis*), which accumulates especially in 10.75 m. CaCO_3 decreases in unit 2 below 30% with lowest values down to 19% in 10.75 m depth, while C_{org} increases in 10.75 m depth to a value of 0.4%. SiO_2 (22%) is lower in unit 2 than in the adjacent units above and below.

The following unit 1 starts at 10 m depth and represents the top section of the profile. It shows similar characteristics than unit 3, with a light brown (7.5YR6.3) in color, CaCO_3 in the range of 40–44% and SiO_2 in the range of 26–36%. C_{org} is in the lower part of unit 1 again very low ($<0.2\%$), but increases steadily up to the surface to a value of 1.4%.

4.2. Chronostratigraphy

OSL analytical data are given in Table 3 for dose rate (\dot{D}) determination. For all samples, no significant radioactive disequilibrium was detected. In Table 2, results for equivalent dose (D_e) and OSL age calculation are listed. Due to a high inter-aliquot scatter (Fuchs and Wagner, 2003), most of the samples show insufficient bleaching and D_e calculation was performed after the method described by Fuchs et al. (2007).

The contents of U, Th and K is expressed by \dot{D} (Table 3). Thereafter, samples from unit 3b show lower values (1.38–1.70 Gy ka^{-1}) than samples from unit 3a (1.95–2.03 Gy ka^{-1}). In unit 2, \dot{D} increases to 2.30–2.43 Gy ka^{-1} , representing the highest values in the entire profile. In unit 1, \dot{D} decreases to values from 1.64–2.07 Gy ka^{-1} . Thus, the overall pattern of dose rate versus sample depth follows the classification in three sedimentary units.

Within errors, the calculated OSL ages are in stratigraphic order (Table 2). With the oldest sample BT 129 at 19.5 m depth, the profile represents the sedimentation cycle of the last 19.16 ± 1.39 ka. In Fig. 5,

Table 3
OSL dating results

Sample no.	Depth (m)	D_e (Gy)	\dot{D} (Gy/ka)	OSL age (ka)
BT 110	0.5	0.60±0.02	1.80±0.10	0.33±0.02
BT 84	1.0	1.89±0.15	1.91±0.10	0.99±0.09
BT 111	1.5	3.01±0.08	2.07±0.11	1.45±0.08
BT 96	2.0	3.76±0.12	1.99±0.10	1.89±0.12
BT 112	2.5	4.86±0.15	2.10±0.11	2.33±0.14
BT 69	3.0	6.92±0.16	1.99±0.10	3.48±0.20
BT 113	3.5	7.43±0.19	2.02±0.10	3.67±0.21
BT 114	4.5	9.69±0.20	2.01±0.10	4.82±0.27
BT 85	5.0	11.07±0.11	2.06±0.11	5.38±0.29
BT 115	5.5	11.36±0.33	2.01±0.11	5.66±0.34
BT 116	6.5	12.06±0.16	1.78±0.10	6.76±0.37
BT 99	7.0	13.62±0.19	1.85±0.10	7.36±0.40
BT 117	7.5	13.33±0.26	1.76±0.10	7.57±0.42
BT 86	8.0	13.21±0.21	1.64±0.11	8.07±0.57
BT 118	8.5	15.19±0.34	1.97±0.13	8.08±0.58
BT 119	9.5	13.77±0.28	1.69±0.12	8.14±0.58
BT 101	10.0	16.36±0.50	1.86±0.13	8.79±0.66
BT 120	10.5	19.24±0.52	2.43±0.17	7.91±0.59
BT 155	10.8	19.15±0.45	2.30±0.16	8.34±0.60
BT 121	11.5	19.98±0.37	2.34±0.16	8.55±0.59
BT 102	12.0	17.02±0.44	1.95±0.13	8.71±0.62
BT 122	12.5	18.94±0.57	1.97±0.14	9.63±0.73
BT 103	13.0	19.39±0.56	1.97±0.14	9.86±0.74
BT 123	13.5	21.46±0.37	2.02±0.14	10.61±0.76
BT 104	14.0	19.24±0.59	2.00±0.14	9.63±0.74
BT 124	14.5	25.38±0.57	2.03±0.14	12.50±0.92
BT 105	15.0	23.36±0.59	1.65±0.11	14.16±1.05
BT 125	15.5	21.02±0.74	1.55±0.11	13.59±1.07
BT 106	16.0	24.33±0.46	1.70±0.12	14.28±1.04
BT 126	16.5	24.42±0.50	1.59±0.11	15.37±1.13
BT 107	17.0	23.13±0.27	1.49±0.11	15.56±1.11
BT 127	17.5	25.16±0.56	1.54±0.11	16.30±1.20
BT 128	18.5	24.42±0.52	1.42±0.10	17.18±1.26
BT 109	19.0	23.10±0.75	1.38±0.10	16.72±1.30
BT 129	19.5	28.86±0.50	1.51±0.11	19.16±1.39

Sample no., sampling depth, as well as equivalent dose (D_e), dose rate (\dot{D}) and OSL ages with their 1σ errors are listed.

the age versus depth plot shows a clear trisection of the sediment profile. This classification is based on sedimentation rates calculated on the base of the OSL ages by linear regression. Thereafter, a sedimentation rate of 0.8 mm a^{-1} ($R^2=0.92$) is characteristic for the period of 19.16 ± 1.39 ka (BT129) to 12.50 ± 0.92 ka (BT124), covering the lower end of the profile to a depth of 14.5 m. Then, the sedimentation rate shortly decreases to 0.2 mm a^{-1} (14.5–14.0 m), before it increases to 3.8 mm a^{-1} ($R^2=0.71$) between 14.0 m and 8.0 m, representing the period between 9.63 ± 0.74 ka (BT104) and 8.07 ± 0.57 ka (BT86). This period can be subdivided, into a late period of pronounced sedimentation between 12 m and 8 m (6.3 mm a^{-1}) from 8.71 ± 0.62 ka (BT102) to 8.07 ± 0.57 ka (BT86), even that the

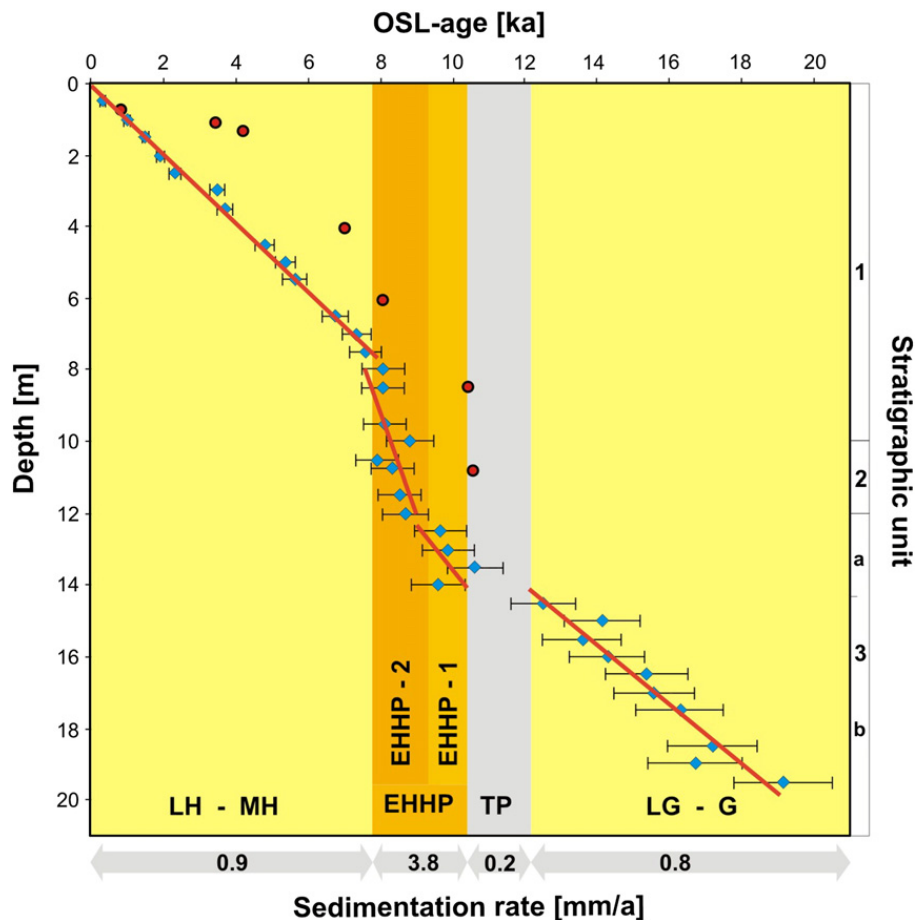


Fig. 5. OSL age versus depth model and the stratigraphical units for the profile Maqta. The OSL ages (diamonds) are given with their 1σ -errors. Additionally, uncorrected ^{14}C ages are given (circles), showing distinct age overestimations due to the *hard-water* effect. OSL ages are grouped according to the change in slope, indicated by the correlation line for each group. Based on the grouping, sedimentation rates are calculated for the Glacial to Lateglacial (G–LG) of ca. 0.8 mm a^{-1} , for the transitional period (TP) of ca. 0.2 mm a^{-1} , the early Holocene moist period (EHHP) of ca. 3.8 mm a^{-1} and the middle to late Holocene (MH–LH) of ca. 0.9 mm a^{-1} . Due to a distinct rise in sedimentation rate at the end of the EHHP, it can be divided in an EHHP-1 and -2.

quality of the regression with $R^2=0.4$ is not very high. At 8 m depth, the sedimentation rate decreases to a value of 0.9 mm a^{-1} ($R^2=0.99$) for the last 8 ka. Thus, sedimentation rates of the lower part of the profile with their changes at 14 m and 12 m depth correlate well with the stratigraphic units 3a, 3b and the beginning of 2.

Table 4
 ^{14}C dating results

Sample no.	Depth (m)	$\delta^{13}\text{C}$ (‰)	Conventional ^{14}C -age (ka)
Poz-3140	0.80	-4.4	825 ± 25 BP
Poz-3141	1.30	0.2	3470 ± 25 BP
Poz-3142	1.60	-2.2	4125 ± 30 BP
Poz-3583	4.00	-2.4	6470 ± 50 BP
Poz-4789	6.00	-5.7	8010 ± 40 BP
Poz-4788	8.50	-2.0	10340 ± 50 BP
Poz-4060	10.75	-0.2	10430 ± 50 BP

Sample no., sampling depth, as well as uncalibrated and calibrated ^{14}C dating results are listed.

However, stratigraphic unit 1 starts at 10 m depth, whereas the change in sedimentation rate is at 7.5 m to 8 m depth. But due to the high sedimentation rate in unit 2, this difference may represent less than 300 a.

Next to the OSL chronology, ^{14}C ages were determined on mollusk remains from the upper part of the profile (Table 4). The uncalibrated ^{14}C -ages show a general trend to much higher ages than the OSL ages. The reason for this ^{14}C -age overestimation is thought to be due to the geology (Cretaceous and Tertiary limestone) and its resulting reservoir and hard-water effect. In addition, ^{14}C -age overestimation might be the consequence of incorporation of old organic material into the younger sedimentary cycle (Lang and Hön-scheidt, 1999). However, due to the mentioned reasons for age overestimation, ^{14}C -ages were not calibrated but they still show the general trend of a sudden increase in sedimentation rate at about 8 m depth (Fig. 5), as demonstrated by the OSL ages.

5. Discussion

5.1. Glacial to Lateglacial

Based on the OSL ages and the calculated sedimentation rates, paleorainfall and the overall paleoenvironmental conditions seemed to be homogeneous in the period from 19.16 ± 1.39 ka to 12.50 ± 0.92 ka. In this period of sediment unit 3b, paleorainfall is interpreted to be low, which is supported by low values of C_{org} as a proxy for the remains of below ground biomass production (low root biomass reflecting low shoot biomass) and high values of $CaCO_3$ as a proxy for low solution and vertical displacement of carbonates. The relatively high sand content in unit 3b could be of eolian origin, thus a proxy for increased wind activity and arid conditions in the nearby source area, which is also supported by a slightly increased SiO_2 content. Thus, the Glacial to Lateglacial is interpreted to be a period of arid conditions, which coincides with previously published data from northern Oman (Burns et al., 2001; Fleitmann et al., 2003), where the absence of speleothem growth indicates aridity. In Yemen (Lézine et al., 2007) and the UAE (Parker et al., 2006), the predominance of arid conditions in this period is indicated by a lack of lacustrine sediments.

5.2. Transitional period

At 12.5 ± 0.92 ka the Glacial to Lateglacial period of unit 3b ends with a short transitional phase of a strongly reduced sedimentation rate, interpreted as a period of even less rainfall than before. This transitional phase (TP) lasts for about 2 ka until the beginning of unit 3a and may represent a period of pronounced aridity, which falls together with the European Younger Dryas. This arid episode is known from IOM influenced Africa (Gasse and Van Compo, 1994; Gasse, 2000), but could so far not be identified on the southern Arabian Peninsula.

5.3. Early Holocene

After the transitional phase of pronounced aridity, sediment unit 3a starts at ca. 10.5 ka with a distinct onset of a humid period, indicated by a sudden increase in sedimentation rate and C_{org} , while $CaCO_3$ decreases. The low content of SiO_2 and sand as an eolian proxy clearly supports the interpretation as a humid period which lasts until about 8 ka.

Within this period of overall humid conditions the episode between ca. 8–9 ka appears as a time of even more pronounced rainfall, where sedimentation rates are highest. Within this period sediments show the highest content of

mollusk remains (*Z. insularis*), a peak in C_{org} and a negative peak in $CaCO_3$. Thus, the early Holocene humid period (EHHP) can be divided in two stages: an early stage EHHP-1 from ca. 10.5–9 ka, where sedimentation rate increases rapidly after the previous arid episode of the transitional phase (TP) and a following stage EHHP-2 from ca. 9–8 ka, where sedimentation rates increase again, showing the most rapid sedimentation in the whole profile.

The onset of the humid period EHHP-1 at about 10.5 ka is confirmed by studies from northern (Burns et al., 2001) and southern Oman (Fleitmann et al., 2003), but its timing differs from that in Yemen (Lézine et al., 2007) with an earlier onset of the humid period at 12 ka, or an even later onset in UAE at 8.5 ka (Parker et al., 2006). However, most of the studies from southern Arabia confirm a period of maximum early Holocene rainfall during the EHHP-2 at 9–8 ka (Cremaschi and Negrino, 2005; Lézine et al., 2007; Fleitmann et al., 2003; Parker et al., 2006).

The 8.2 ka event as a short interval of reduced rainfall within the overall humid period, which was identified in studies on speleothems from north and south Oman (Fleitmann et al., 2003, 2007), was not detected in the sediment archive from Maqta. This may be due to the less sensitive sediment archive at Maqta, with large errors for the OSL ages. However, Neff et al. (2001) identified an increase in stalagmite growth rate in northern Oman during 8–8.2 ka, which is often used as a proxy for enhanced precipitation (Polyak and Asmerom, 2001; Fleitmann et al., 2004) and would thus confirm the results from Maqta.

5.4. Mid-late Holocene

After the EHHP at ca. 8 ka, the sedimentation rate is decreasing to a relatively constant value of ca. 0.9 mm a^{-1} , which is representative for the middle to late Holocene. This period is interpreted as relatively arid, which is also documented in a decreasing content of C_{org} and an increasing content of $CaCO_3$ and SiO_2 . However, the change from high to lower sedimentation rates at about 8 ka is shown at the depth of 8 m, whereas the change in the sediment characteristic from unit 2 to unit 1 takes place at a depth of 10 m. Within errors the OSL ages from 8 m and 10 m are the same and both changes take place at about 8 ka. Based on an average sedimentation rate for the EHHP-2 of ca. 6.3 mm a^{-1} , there is an age difference probably of ≤ 300 a.

The transition from the EHHP to the following arid period at about 8 ka correlates within uncertainties of the age model with the findings from Lézine et al. (2007)

in Yemen and also with data from southern Oman (Fleitmann et al., 2003), where a gradual long-term decrease in precipitation is seen since about 8 ka. In contrast, Radies et al. (2005) identified the beginning of the arid period in southern Oman at 5.5 ka and in northern Oman, Burns et al. (2001) identified the reduction in rainfall at ca. 6 ka. Even further north in the UAE, Bray and Stokes (2004) and Parker et al. (2006) identified the beginning of the arid period also at 6 ka.

5.5. The ITCZ shift

Variations of paleorainfall in the southern part of the Arabian Peninsula are generally explained by variations in the strength of the IOM and the associated boreal summer position of the ITCZ (Fleitmann et al., 2007; Overpeck et al., 1996). During the Glacial and Lateglacial, the position of the ITCZ was supposed to be south of the Arabian Peninsula and the SW monsoon was unable to effect southern Arabia. The following northward shift of the ITCZ at the early Holocene caused the onset of the humid period, whereas its termination is associated with a southward shift of the ITCZ to its present-day position along the southern coast of the Arabian Peninsula.

Thereafter, the ITCZ reached Maqta in northern Oman (23°N) at about 10.5 ka, which is in accordance with data from Burns et al. (2001) and Fleitmann et al. (2003). An even further northward shift might be reached at ca. 8.5 ka in the UAE (Parker et al., 2006). This timing of the northward shift of the ITCZ differs from data given by Overpeck et al. (1996) or Lézine et al. (2007), which indicate an earlier shift of the ITCZ, whereas the data given by Radies et al. (2005) would imply an even later northward migration. However, most of the data show a humid period on the southern Arabian Peninsula at ca. 9–8 ka (EHHP-2), indicating that at that time the ITCZ was approximately at a latitudinal position of the UAE.

The evident decrease in rainfall at Maqta after the EHHP at ca. 8 ka indicates a southward shift of the ITCZ, which is in accordance with results from Lézine et al. (2007). Due to the gradual decrease in rainfall after 7.6 ka in southern Oman (Fleitmann et al., 2003, 2007), the position of the ITCZ supposedly migrated gradually southward to a position south of the Arabian Peninsula. In contrast, data from Burns et al. (2001) show a termination of the EHHP in northern Oman at ca. 6 ka, indicating a later southward shift of the ITCZ. However, the abrupt decrease in sedimentation rate at about 8 ka in Maqta, indicating a sudden decrease in rainfall, might be explained by the threshold concept (Coates and Vitek, 1980). Rainfall intensities below a certain threshold may not produce enough surface run-off to erode and transport sufficient sediment. Thus, a gradual

decrease in rainfall might not be seen in the evolution of the sedimentation rate.

Onset, duration and temporal characteristic of arid and humid periods throughout the southern Arabian Peninsula and its associated positions of the ITCZ are still under debate. The partially contrary results from various studies might be due to dating problems or differences in the sensitivity and characteristic of the natural archives recording the climate signals. These differences may also indicate a much more complicated pattern of rain bringing atmospheric conditions at a local scale, which can only be partially explained by the general large scale model of the northern and southern shift of the ITCZ and its associated SW monsoon. Especially in times of climatic transition and a more northerly position of the ITCZ, thunderstorms originating from the Gulf of Oman may have played a more prominent role as a source of precipitation and subsequent erosion–sedimentation events than nowadays.

6. Conclusions

Based on OSL ages, the calculated sedimentation rates from the sediment record from Maqta in northern Oman represent a valuable proxy for paleorainfall of the last 20 ka, which was confirmed by additional chemical analyses of the sediments. The key inferences are:

- (1) The Glacial to Lateglacial period seems to be characterized by a homogeneous sedimentation rate, lasting from 9.16 ka to 12.50 ka. During this period, rainfall was low, indicating arid conditions.
- (2) The following transitional period from 12.5 ka to 10.5 ka shows a decreasing sedimentation rate, indicating a period of strongly reduced rainfall. This period might be correlated with the European Younger Dryas cooling event, so far not found in records from southern Arabia.
- (3) An abrupt increase in sedimentation rates (rainfall) at about 10.5 ka indicates the onset of the early Holocene humid period (EHHP), which lasts until about 8 ka. An even higher sedimentation rate from 9–8 ka indicates a maximum in rainfall within the EHHP.
- (4) After 8 ka, sedimentation rates decrease, showing a decrease in rainfall and indicating arid conditions for the middle and late Holocene.

The onset and termination of the arid and humid periods in southern Arabia are related to the position of the ITCZ and its associated SW monsoon pattern. Due to the presented data and based on several studies from southern Arabia, a rapid northward shift of the ITCZ at

about 10.5 ka may have caused the onset of the early Holocene humid period (EHHP), whereas its termination at 8 ka could be associated with a southward migrating of the ITCZ. However, discrepancies of the onset and termination of the arid and humid periods between the various studies from southern Arabia still exist, which might be due to differences in the sensitivity of the investigated archives or in a more complex pattern of the atmospheric conditions at a local scale.

Acknowledgements

We would like to thank Manfred Fischer from the University of Bayreuth for luminescence sample preparation, and Detlef Degering from the Saxonian Academy of Science for low-level γ -spectrometry measurements. Hans von Suchodoletz from University of Bayreuth is thanked for the semi-quantitative quartz analysis, Eva Wiegard and Claudia Thieme from University of Kassel-Witzenhausen for soil chemical analyses and Eike Luedeling for constructing the topographic model of the northern Oman mountains in Fig. 2. The authors are indebted to Rashid bin Ahmad Al-Uwaysi and the farmers of Maqta for their help in digging the 20 m pit and during the taking of samples during several day and night sampling periods, to Sulaiman Al Khanjari and Horst Weier for his advice, to Sultan Qaboos University at Muscat for infrastructural support and to the Deutsche Forschungsgemeinschaft (DFG) for funding (BU1308).

References

- Aitken, M., 1998. *An Introduction to Optical Dating*. Oxford University Press, Oxford.
- Andrews, J.E., Singhvi, A.K., Kailath, A.J., Kuhn, R., Dennis, P.F., Tandon, S.K., Dhir, R.P., 1998. Do stable isotope data from calcareous record late Pleistocene monsoonal climate variation in the Thar Desert of India? *Quat. Res.* 50, 240–251.
- Bray, H.E., Stokes, S., 2004. Temporal patterns of arid–humid transitions in the south-eastern Arabian Peninsula based on optical dating. *Geomorphology* 59, 271–280.
- Burns, S.J., Fleitmann, D., Matter, A., Neff, U., Mangini, A., 2001. Speleothem evidence from Oman for continental pluvial events during interglacial periods. *Geology* 29, 623–626.
- Chase, B., Thomas, D., 2007. Multiphase late Quaternary aeolian sediment accumulation in western South Africa: timing and relationship to palaeoclimatic changes inferred from the marine record. *Quat. Int.* 166, 29–41.
- Coates, D.R., Vitek, J. (Eds.), 1980. *Thresholds in Geomorphology*. George Allen & Unwin, London.
- Cremschi, M., Negrino, F., 2005. Evidence for an abrupt climatic change at 8700 ^{14}C yr B.P. Rockshelters and Caves of Gebel Qara (Dhofar-Oman): Palaeoenvironmental Implications. *Geoarchaeology*, vol. 20, pp. 559–579.
- Crombie, M.K., Arvidson, R.E., Sturchio, N.C., El Alf, Z., Abu Zeid, K., 1997. Age and isotopic constraints on Pleistocene pluvial episodes in the Western Desert, Egypt. *Palaeogeogr. Palaeoclimatol. Palaeoecol.* 130, 337–355.
- DeMenocal, P., Ortiz, J., Guilderson, T., Adkins, J., Sarnthein, M., Baker, L., Yarusinsky, M., 2000. Abrupt onset and termination of the African Humid Period: rapid climate responses to gradual insolation forcing. *Quat. Sci. Rev.* 19, 347–361.
- Eitel, B., Blümel, W.D., Hüser, K., Mauz, B., 2001. Dust and loessic alluvial deposits in northwestern Namibia (Damaraland, Kaokoveld): sedimentology and palaeoclimatic evidence based on luminescence data. *Quat. Int.* 76/77, 57–65.
- Eitel, B., Kadereit, A., Blümel, W.D., Hüser, K., Kromer, B., 2005. The Amspoort Silts, northern Namib Desert (Namibia): formation, age and palaeoclimatic evidence of river-end deposits. *Geomorphology* 64, 299–314.
- Eitel, B., Kadereit, A., Blümel, W.-D., Hüser, K., Lomax, J., Hilgers, A., 2006. Environmental changes at the eastern Namib Desert margin before and after the Last Glacial Maximum: new evidence from fluvial deposits in the upper Hoanib River catchment, northwestern Namibia. *Palaeogeogr. Palaeoclimatol. Palaeoecol.* 234, 201–222.
- Fleitmann, D., Burns, S.J., Mudelsee, M., Neff, U., Kramers, J., Mangini, A., Matter, A., 2003. Holocene forcing of the Indian Monsoon recorded in a stalagmite from southern Oman. *Science* 300, 1737–1739.
- Fleitmann, D., Burns, S.J., Neff, U., Mudelsee, M., Mangini, A., Matter, A., 2004. Palaeoclimatic interpretation of high-resolution oxygen isotope profiles derived from annually laminated speleothems from Southern Oman. *Quat. Sci. Rev.* 23, 935–945.
- Fleitmann, D., Burns, S.J., Mangini, A., Mudelsee, M., Kramers, J., Villa, I., Neff, U., Al-Subbary, A.A., Buettner, A., Hippler, D., Matter, A., 2007. Holocene ITCZ and Indian monsoon dynamics recorded in stalagmites from Oman and Yemen (Socotra). *Quat. Sci. Rev.* 26, 170–188.
- Fuchs, M., Wagner, G.A., 2003. Recognition of insufficient bleaching by small aliquots of quartz for reconstructing soil erosion in Greece. *Quat. Sci. Rev.* 22, 1161–1167.
- Fuchs, M., Woda, C., Bürkert, A., 2007. Chronostratigraphy of a sediment record from the Hajar mountain range in north Oman: implications for optical dating of insufficiently bleached sediments. *Quat. Geochronol.* 2, 202–207.
- Gasse, F., 2000. Hydrological changes in the African tropics since the Last Glacial Maximum. *Quat. Sci. Rev.* 19, 189–211.
- Gasse, F., Van Campo, E., 1994. Abrupt post-glacial climate events in West Asia and North Africa monsoon domains. *Earth Planet. Sci. Lett.* 126, 435–456.
- Gee, G.W., Bauder, J.W., 1986. Particle size analysis. In: Klute, A. (Ed.), *Methods of Soil Analysis. Part 1. Physical and Mineralogical Methods*. 2nd ed. Agron. Monogr. 9. ASA and SSSA, Madison, WI.
- Glennie, K.W., Singhvi, A.K., 2002. Event stratigraphy, paleoenvironment and chronology of SE Arabian deserts. *Quat. Sci. Rev.* 21, 853–869.
- Heine, K., 2004. Little Ice Age climatic fluctuations in the Namib Desert, Namibia, and adjacent areas: evidence of exceptionally large floods from slack water deposits and desert soil sequences. *Lect. Notes Earth Sci.* 102, 137–165.
- Juyal, N., Chamyal, L.S., Bhandari, S., Bushan, R., Singhvi, A.K., 2006. Continental record of the southwest monsoon during the last 130 ka: evidence from the southern margin of the Thar Desert, India. *Quat. Sci. Rev.* 25, 2632–2650.

- Kröpelin, S., Soulié-Märsche, I., 1991. Charophyte remains from Wadi Howar as evidence for deep Mid-Holocene Freshwater Lakes in the Eastern Sahara of Northwest Sudan. *Quat. Res.* 36, 210–223.
- Kuper, R., Kröpelin, S., 2006. Climate-controlled Holocene occupation in the Sahara: motor of Africa's evolution. *Science* 313, 803–807.
- Lang, A., Hönscheidt, S., 1999. Age and source of colluvial sediments at Vaihingen-Enz, Germany. *Catena* 38, 89–107.
- Leuschner, D.C., Sirocko, F., 2000. The low-latitude monsoon climate during Dansgaard-Oeschger cycles and Heinrich Events. *Quat. Sci. Rev.* 19, 243–254.
- Lézine, A.-M., Tiercelin, J.-J., Robert, C., Saliège, J.-F., Cleuziou, S., Inizan, M.-L., Braemer, F., 2007. Centennial to millennial-scale variability of the Indian monsoon during the early Holocene from a sediment, pollen and isotope record from the desert of Yemen. *Palaeogeogr. Palaeoclimatol. Palaeoecol.* 243, 235–249.
- Munsell Color Corporation, 1976. *Munsell Book of Color-Matte Finish Collection*. Baltimore, MD, USA.
- Murray, A., Wintle, A., 2000. Luminescence dating of quartz using an improved single-aliquot regenerative-dose protocol. *Radiat. Meas.* 32, 57–73.
- Neff, U., Burns, S.J., Mangini, A., Mudelsee, M., Fleitmann, D., Matter, A., 2001. Strong coherency between solar variability and the monsoon in Oman between 9 and 6 kyr ago. *Nature* 411, 290–293.
- Overpeck, J., Anderson, D., Trumbore, S., Warren, P., 1996. The southwest Indian Monsoon over the last 18000 years. *Clim. Dyn.* 12, 213–225.
- Page, A.L., Miller, R.H., Kennedy, D.R. (Eds.), 1982. *Methods of Soil Analysis. Part 2. Chemical and Microbiological Properties*, 2nd ed. Agronomy Series, vol. 9. ASA, SSSA, Madison, Wis., U.S.A.
- Parker, A.G., Goudie, A.S., Stokes, S., White, K., Hodson, M.J., Manning, M., Kennet, D., 2006. A record of Holocene climate change from lake geochemical analyses in southeastern Arabia. *Quat. Res.* 66, 465–476.
- Polyak, V.J., Asmerom, Y., 2001. Late Holocene climate and cultural changes in the southwestern United States. *Science* 294, 148–151.
- Prescott, J.R., Hutton, J.T., 1994. Cosmic ray contributions to dose rates for luminescence and esr dating: large depths and long-term time variations. *Radiat. Meas.* 23, 497–500.
- Preusser, F., Radies, D., Matter, A., 2002. A 160,000-year record of dune development and atmospheric circulation in Southern Arabia. *Science* 296, 2018–2020.
- Radies, D., Preusser, F., Matter, A., Mange, M., 2004. Eustatic and climatic controls on the development of the Wahiba Sand Sea, Sultanate of Oman. *Sedimentology* 51, 1359–1385.
- Radies, D., Hasiotis, S.T., Preusse, F., Neubert, E., Matter, A., 2005. Paleoclimatic significance of the Early Holocene faunal assemblages in wet interdune depositions of the Wahiba Sand Sea, Sultanate of Oman. *J. Arid Environ.* 62, 109–125.
- Sirocko, F., Samthei, M., Erlenkeuser, H., Lange, H., Arnold, M., Duplessy, J.C., 1993. Century-scale events in monsoonal climate over the past 24,000 years. *Nature* 364, 322–324.
- VDLUFA, 1991. *German Agricultural Testing and Research Agency. Book of Methods, Vol. 1 (1991), Soil Exploration, Method A 5.3.1.*
- Weyhenmeyer, C.E., Burns, S.J., Waber, H.N., Aeschbach-Hertig, W., Kipfer, R., Loosli, H.H., Matter, A., 2000. Cool glacial temperature and changes in moisture source recorded in Oman groundwaters. *Science* 287, 842–845.